Unimolecular Decompositions of Ionized Isopropyl Methyl Ether: An ab Initio and RRKM Study

Santiago Olivella,*,† Albert Solé,† David J. McAdoo,*,‡ and Lawrence L. Griffin§

Contribution from the Departaments de Química Orgànica i Química Física, Universitat de Barcelona, Martí i Franquès 1, 08028 Barcelona, Catalunya, Spain, Marine Biomedical Institute, University of Texas Medical Branch, Galveston, Texas 77555-0843, and Department of Marine Sciences, Texas A&M University at Galveston, Galveston, Texas 77553

Received October 14, 1994⊗

Abstract: In connection with the unimolecular decompositions of ionized isopropyl methyl ether, namely, methane elimination and methyl radical loss, ab initio molecular orbital calculations at the UMP2, QCISD, and QCISD(T) levels of theory with the 6-31G(d) and 6-31G(d,p) basis sets have been used to investigate the relevant parts of the $C_4H_{10}O^{\bullet+}$ ground-state potential energy surface. The calculations demonstrate that at internal energies below the threshold for loss of a methyl radical, bond dissociation to an ion−neutral complex, $[CH_3O^+{=}CHCH_3\ CH_3^\bullet]$, and methane elimination therefrom both occur. Sets of reactant and transition state frequencies calculated at the UMP2/6-31G(d) level, as well as energetics based on QCISD(T)/6-31G(d,p)//UMP2/6-31G(d) + ZPVE calculations, were employed in RRKM calculations. By invoking quantum-mechanical barrier tunneling in the methane elimination channel, we were able to reproduce several experimental observations: (a) the methane elimination reaction dominates at internal energies near the threshold for dissociation; (b) the onsets for the methane and methyl losses differ by only a few tenths of a kilocalorie per mole; and (c) there is a very strong primary isotope effect of about 60 on the CH_2D_2 and CHD_3 losses from $CH_3OCH(CHD_2)_2^{\bullet+}$.

Introduction

The unimolecular chemistry of ionized ethers in the gas phase has been the subject of continuous experimental and theoretical research.[1] In particular, the unimolecular decomposition reactions of ionized isopropyl methyl ether (**1**) have been studied in detail.[2] Upon electron-impact ionization, photoionization, and collisional activation, **1** dissociates by losing one of the carbon-bound methyls to give $CH_3O^+{=}CHCH_3$ as the dominant (>99%) product. By contrast, the metastable isopropyl methyl ether radical cation ($\mathbf{1}^{\bullet+}$) eliminates competitively CH_4 and $CH_3^\bullet$, in a proportion that depends on pressure (Scheme 1).[2,3] Photoionization appearance energy measurements gave almost identical values for the products of CH_4 and $CH_3^\bullet$ eliminations (9.69 and 9.71 eV, respectively), *ca* 0.2 eV above the ionization energy of **1** (9.50 eV). The very small average translational energy ($\langle T\rangle$) released in the $CH_3^\bullet$ elimination (0.2 kcal/mol) demonstrated that this dissociation takes place at its thermochemical threshold, whereas the larger $\langle T\rangle$ value (1 kcal/mol) determined for the CH_4 elimination suggested that this decomposition may have a small reverse activation energy. Deuterium labeling studies[2] (Scheme 2) established that there are very strong primary isotope effects on the metastable methane losses, as D_4-labeled $\mathbf{1}^{\bullet+}$ ($\mathbf{1a}^{\bullet+}$) loses CH_2D_2 30 times more frequently than it loses CHD_3. Correcting for the 2:1 D:H availability gives a primary isotope effect of 60. The competing elimination of CH_4 and $CH_3^\bullet$ and the rapid switching between these two decompositions near the threshold for simple dissociation have been attributed[2] to the involvement of an ion−neutral complex, i.e., a species in which noncovalent interactions retain close together two entities formed by simple bond cleavages, so that they are able to react unimolecularly (e.g., an incipient cation may isomerize) or bimolecularly (e.g., by hydrogen atom transfer).[4] An alternative mechanism involving a classical, i.e., bond-making−bond-breaking, rearrangement has also been suggested.[3]

Scheme 1

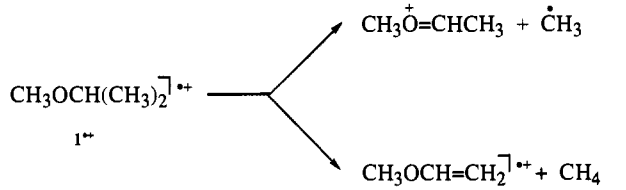

Scheme 2

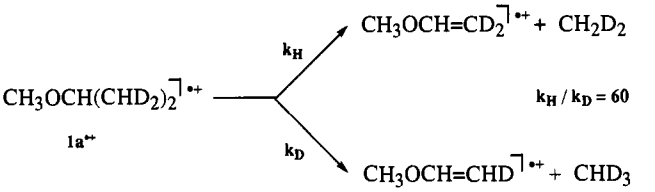

In this article, we address the questions related to the mechanism of $CH_3^\bullet$ and CH_4 losses from ionized **1**. Specifically: (a) What is the equilibrium geometry of the ground state ion $\mathbf{1}^{\bullet+}$? (b) Does an ion−neutral complex mediate the decomposition modes of ionized **1**, and if this turns out to be the case, at what point does the $CH_3^\bullet$ become free enough that

† Universitat de Barcelona.
‡ University of Texas Medical Branch.
§ Texas A&M University.
⊗ Abstract published in *Advance ACS Abstracts*, February 15, 1995.

(1) For a recent review see: Turecek, F. In *The Chemistry of Hydroxyl, Ether and Peroxide Groups*; Patai, S., Ed.; John Wiley: New York, 1993; Vol. 2, Suppl. E.

(2) McAdoo, D. J.; Traeger, J. C.; Hudson, C. E.; Griffin, L. L. *J. Phys. Chem.* **1988**, *92*, 1524.

(3) Weiske, T.; Akkök, S.; Schwarz, H. *Int. J. Mass Spectrom. Ion Proc.* **1987**, *76*, 117.

(4) (a) Morton, T. H. *Tetrahedron* **1982**, *38*, 3195. (b) McAdoo, D. J. *Mass Spectrom. Rev.* **1988**, *7*, 363. (c) Bouchoux, G. *Adv. Mass Spectrom.* **1989**, *11*, 812. (d) Hammerum, S. In *Fundamentals of Gas Phase Ion Chemistry*; Jennings, K. R., Ed.; Kluwer Academic Publishers: Dordrecht, The Netherlands, 1990; pp 379−390. Bowen, R. D. *Acc. Chem. Res.* **1991**, *24*, 364. (e) Longevialle, P. *Mass Spectrom. Rev.* **1992**, *11*, 157. (f) McAdoo, D. J.; Morton, T. H. *Acc. Chem. Res.* **1993**, *26*, 295.

0002-7863/95/1517-2557$09.00/0

Table 1. Calculated Total Energies (hartrees) and Zero-Point Vibrational Energies (ZPVE, kcal/mol)[a] for MP2/6-31G(d) Optimized Structures

structure	point group	state	n.i.f.[b]	UMP2/6-31G(d)	UMP2[c]/6-31G(d,p)	QCISD[c]/6-31G(d,p)	QCISD(T)[c]/6-31G(d,p)	ZPVE
I	C_S	$^1A'$	0	−232.863 37	−232.922 46	−232.982 37	−233.004 59	82.0
II	C_S	$^2A''$	1	−232.517 89	−232.573 70	−232.647 49	−232.669 57	80.0
III	C_1	^2A	0	−232.518 97	−231.574 67	−232.647 84	−232.670 42	79.9
IV	C_1	^2A	1	−232.509 14	−232.564 91	−232.631 42	−232.651 63	77.0
V	C_1	^2A	0	−232.509 34	−232.565 04	−232.631 55	−232.651 83	77.1
VI	C_S	$^1A'$	0	−192.829 63	−192.865 90	−192.911 66	−192.929 04	58.0
VII	C_1	^2A	1	−232.498 45	−232.555 69	−232.619 69	−232.642 60	76.2
VIII	C_1	^2A	0	−232.524 93	−232.581 22	−232.648 37	−232.668 77	78.2
IX	C_S	$^2A''$	0	−192.184 47	−192.213 04	−192.259 05	−192.275 66	50.6
X	C_1	^2A	1	−232.478 12	−232.535 96	−232.602 99	−232.625 96	75.3
XI	C_S	$^2A''$	0	−192.166 76	−192.195 28	−192.242 45	−192.259 98	49.3
$CH_3^\bullet$	D_{3h}	$^2A_2''$	0	−39.673 03	−39.692 67	−39.713 72	−39.716 23	17.8
CH_4	T_d	$^1A_1$	0	−40.337 04	−40.364 58	−40.386 12	−40.389 59	27.1

[a] Calculated using MP2/6-31G(d) vibrational frequencies, scaled by 0.93. [b] Number of imaginary frequencies. [c] In the frozen core approximation.

an ion−neutral complex is formed, and where is this point in relation to the transition state for H-transfer to the $CH_3^\bullet$? (c) Why is methane elimination confined to a very narrow energy range? (d) Why are the experimental thresholds for the losses of $CH_3^\bullet$ and CH_4 virtually identical? (e) Where do the very large isotope effects come from? To respond to these questions, we investigated the stationary points on the $C_4H_{10}O^{\bullet+}$ ground-state potential energy surface (PES) most relevant to the $CH_3^\bullet$ and CH_4 losses from $\mathbf{1}^{\bullet+}$ by means of ab initio molecular orbital calculations. The energetic, structural, and vibrational results furnished by these calculations were subsequently used to perform RRKM calculations to predict the rate constants of the competing elimination of CH_4 and $CH_3^\bullet$ from $\mathbf{1}^{\bullet+}$ and the deuterium isotope effects on the CH_2D_2 and CHD_3 losses from $\mathbf{1a}^{\bullet+}$. Comparison between these predictions and the available experimental data provides a reliable test of the decomposition mechanism inferred from the computed PES.

Ab Initio Computational Details

The geometries of the relevant stationary points on the $C_4H_{10}O^{\bullet+}$ ground-state PES were initially located at the spin-unrestricted Hartree−Fock level of theory[5] employing the split-valence d-polarized 6-31G(d) basis set[6] (UHF/6-31G(d)) and then further optimized at the UMP2/6-31G(d) level, where the effects of dynamical electron correlation were accounted for through full (i.e., not frozen core) second-order Møller−Plesset perturbation theory.[7] The amount of spin contamination in the reference UHF wave function was found to be very small; thus the expectation values of the $\hat{S}^2$ operator were always very close to the value of 0.75 for a pure doublet state, i.e., in a range of 0.7599 to 0.7832. At the UMP2/6-31G(d) level, the harmonic vibrational frequencies were obtained by diagonalizing the mass-weighted Cartesian force constant matrix, calculated from analytical second derivatives of the total energy, to characterize the stationary points as minima or as saddle points and to facilitate zero-point vibrational energy (ZPVE) corrections to the relative energies. In order to predict more reliable ZPVE values, the raw theoretical harmonic frequencies were scaled by 0.93 to account for their average overestimation at the UMP2/6-31G(d) level of theory.[8]

Equilibrium geometries were fully optimized within appropriate symmetry constraints using analytical gradient methods.[9] Starting geometries for the transition-structure optimizations were obtained by the usual reaction-coordinate method, the energy being minimized with respect to all other geometrical variables for successive increments in the reaction coordinate. The approximate transition structures located in this way were refined by minimizing the scalar gradient of the energy, using Schlegel's algorithm.[9] The optimized geometries were checked for the correct number of imaginary eigenvalues of the force constant matrix.

At geometries optimized using the UMP2/6-31G(d) wave function, the energies were recalculated using (frozen core) quadratic configuration interaction with the singles, doubles, and perturbative estimation of triples method[10] (QCISD(T)) employing the split-valence d,p-polarized 6-31G(d,p) basis set.[6] Our best relative energies correspond to the QCISD(T)/6-31G(d,p) level together with the ZPVE correction calculated at the UMP2/6-31G(d) level. Unless otherwise noted, these are the values given in the text.

Basis set superposition errors (BSSE) are expected to affect the computed interaction in electrostatically bound species.[11] However, it has been shown that these effects, although they tend to overestimate the ion−neutral complex stability relative to that of the completely separated components, are not very pronounced and do not exceed 1−2 kcal/mol.[12]

The charge and spin density distributions of the most relevant structures were examined by means of the Mulliken population analysis[13] of the **Z** density matrix obtained from UMP2 (full) gradient calculations with the 6-31G(d,p) basis set, an effective correlated density matrix which represents the response of the correlated system to any one-electron perturbation.[14]

All of the ab initio calculations described here were performed with the GAUSSIAN 90[15] and GAUSSIAN 92[16] series of programs, running on a CRAY Y-MP8/864 computer at the CHPC in Austin and a CRAY Y-MP2/32 computer at the CESCA in Barcelona.

Results and Discussion of the Ab Initio Calculations

The most relevant geometrical parameters of the optimized molecular structures are given in Figures 1−7 (bond lengths in angstroms), which are computer plots of the UMP2/6-31G(d)-optimized geometries. The full optimized geometries are

(5) Pople, J. A.; Nesbet, R. K. *J. Chem. Phys.* **1954**, *22*, 571.
(6) Hariharan, P. C.; Pople, J. A. *Theor. Chim. Acta* **1973**, *28*, 213.
(7) (a) Moller, C.; Plesset, M. *Phys. Rev.* **1934**, *46*, 618. (b) Pople, J. A.; Binkley, J. S.; Seeger, R. *Int. J. Quantum Chem., Symp.* **1976**, *10*, 1.
(8) (a) Hout, R. F.; Levi, B. A.; Hehre, W. J. *J. Comput. Chem.* **1982**, *3*, 234. (b) DeFrees, D. J.; McLean, A. D. *J. Chem. Phys.* **1985**, *82*, 333.
(9) Schlegel, H. B. *J. Comput. Chem.* **1982**, *3*, 214.
(10) Pople, J. A.; Head-Gordon, M.; Raghavachari, K. *J. Chem. Phys.* **1987**, *87*, 5968.
(11) See, for example: (a) Urban, M.; P. Hozba, P. *Theor. Chim. Acta* **1975**, *36*, 215. (b) Ostlund, N. S.; Merrifield, D. L. *Chem. Phys. Lett.* **1976**, *39*, 612. (c) Bulski, H.; Chalasinski, G. *Theor. Chim. Acta* **1977**, *44*, 399. (d) Kolos, W. *Theor. Chim. Acta* **1979**, *51*, 219. (e) Leclercq, J. M.; Allavena, M.; Bouteilleur, Y. *J. Chem. Phys.* **1983**, *78*, 4606. (f) Hobza, P.; Zahradnik, R. *Int. J. Quantum Chem.* **1983**, *23*, 325. (g) Wells, B. H.; Wilson, S. *Chem. Phys. Lett.* **1983**, *101*, 429.
(12) (a) Latajka, Z.; Scheiner, S. *Chem. Phys.* **1985**, *98*, 59. (b) Postma, R.; Ruttink, P. J. A.; van Baar, B.; Terlouw, J. K.; Holmes, J. L.; Burgers, P. C. *Chem. Phys. Lett.* **1986**, *123*, 409.
(13) Mulliken, R. S. *J. Chem. Phys.* **1955**, *23*, 1833.
(14) See, for example: Wiberg, K. B.; Hadad, C. M.; LePage, T.; Breneman, C. M.; Frisch, M. J. *J. Phys. Chem.* **1992**, *96*, 671.
(15) Frisch, M. J.; Head-Gordon, M.; Trucks, G. W.; Foresman, J. B.; Schlegel, H. B.; Raghavachari, K.; Robb, M.; Binkley, J. S.; Gonzalez, C.; Defrees, D. J.; Fox, D. J.; Whiteside, R. A.; Seeger, R.; Melius, C. F.; Baker, J.; Martin, R. L.; Kahn, L. R.; Stewart, J. J. P.; Topiol, S.; Pople, J. A. *GAUSSIAN 90*; Gaussian Inc.: Pittsburgh, PA, 1990.
(16) Frisch, M. J.; Trucks, G. W.; Head-Gordon, M.; Gill, P. M. W.; Wong, M. W.; Foresman, J. B.; Johnson, B. G.; Schlegel, H. B.; Robb, M. A.; Replogle, E. S.; Gomperts, R.; Andres, J. L.; Raghavachari, K.; Binkley, J. S.; Gonzalez, C.; Martin, R. L.; Fox, D. J.; Defrees, D. J.; Baker, J.; Stewart, J. J. P.; Pople, J. A. *GAUSSIAN 92*; Gaussian, Inc.: Pittsburgh, PA, 1992.

Table 2. Calculated Relative Energies (kcal/mol) for MP2/6-31G(d)-Optimized Stationary Points on the $C_4H_{10}O^{\bullet+}$ Potential Energy Surface

stationary point	UMP2/6-31G(d)	UMP2[a]/6-31G(d,p)	QCISD[a]/6-31G(d,p)	QCISD(T)[a]/6-31G(d,p)	QCISD(T)[a]/6-31G(d,p) + ZPVE	exp
III	0.0	0.0	0.0	0.0	0.0	0.0
IV	6.2	6.1	10.3	11.8	8.9	
V	6.0	6.0	10.2	11.7	8.9	
VI + $CH_3^{\bullet}$	9.0	10.1	14.1	15.8	11.7	9.6[b]
VII	12.9	11.9	17.7	17.5	13.8	9.3[c]
VIII	−3.7	−4.1	−0.3	1.0	−0.7	
IX + CH_4	−1.6	−1.8	1.7	3.2	1.0	3.5[d]
X	25.6	24.3	28.1	27.9	23.8	
XI + CH_4	9.5	9.3	12.1	13.1	9.5	

[a] In the frozen core approximation. [b] See ref 18. [c] See ref 21. [d] See ref 20.

Table 3. Calculated Total Atomic Charges for MP2/6-31G(d)-Optimized Structures[a,b]

atom	**III**	**V**	**VI** + $CH_3^{\bullet}$	**VIII**	**IX** + CH_4
C1	−0.394	−0.484	−0.482	−0.189	−0.192
C2	+0.039	+0.328	+0.341	+0.286	+0.284
O3	−0.188	−0.281	−0.288	−0.310	−0.310
C4	−0.154	−0.147	−0.150	−0.150	−0.150
H5	+0.200	+0.227	+0.203	+0.118	+0.166
H6	+0.165	+0.222	+0.242	+0.230	+0.233
H7	+0.180	+0.222	+0.242	+0.247	+0.249
H8	+0.237	+0.250	+0.250	+0.255	+0.258
H9	+0.202	+0.203	+0.205	+0.195	+0.198
H10	+0.241	+0.229	+0.233	+0.231	+0.233
H11	+0.236	+0.195	+0.205	+0.197	+0.198
C12	−0.350	−0.415	−0.375	−0.497	−0.663
H13	+0.173	+0.149	+0.125	+0.105	+0.166
H14	+0.200	+0.149	+0.125	+0.179	+0.166
H15	+0.209	+0.152	+0.125	+0.104	+0.166

[a] Determined from the Mulliken population analysis of the **Z** density matrix obtained from UMP2(full)/6-31G(d,p) gradient calculations. [b] Atom numberings refers to Figures 2, 4, and 6.

Table 4. Calculated Total Atomic Spin Densities for MP2/6-31G(d)-Optimized Structures[a,b]

atom	**III**	**V**	$CH_3^{\bullet}$	**VIII**	**IX**
C1	+0.008	+0.006		+0.812	+0.814
C2	−0.004	0.000		+0.083	+0.088
O3	+0.746	+0.001		+0.191	+0.188
C4	−0.036	+0.003		−0.014	−0.014
H5	0.000	+0.016		0.000	
H6	+0.001	0.000		−0.041	−0.041
H7	+0.004	0.000		−0.043	−0.043
H8	+0.030	0.000		−0.009	−0.009
H9	+0.021	0.000		+0.009	+0.009
H10	+0.070	0.000		0.000	−0.001
H11	+0.008	+0.010		+0.009	+0.009
C12	+0.143	+1.137	+1.198	+0.001	
H13	−0.006	−0.057	−0.066	0.000	
H14	−0.008	−0.058	−0.066	+0.003	
H15	+0.023	−0.057	−0.066	0.000	

[a] Determined from the Mulliken population analysis of the **Z** density matrix obtained from UMP2(full)/6-31G(d,p) gradient calculations. [b] Atom numberings refers to Figures 2, 4, and 6.

available as supplementary material. Total energies calculated at various levels of theory are given in Table 1, which includes the ZPVE computed from the scaled vibrational frequencies. Relative energies are collected in Tables 2, together with experimental data derived from known heats of formation or appearance energy measurements. The total atomic charges and spin densities of the most relevant structures are shown in Tables 3 and 4, respectively. Finally, Figure 8 provides a schematic potential energy diagram based on the relative energies calculated at the QCISD(T)/6-31G(d,p)+ZPVE level.

We are unaware of any previous theoretical study of either neutral **1** or $\mathbf{1}^{\bullet+}$. Our lowest-energy equilibrium geometry of **1** corresponds to the C_s structure **I** (Figure 1). The highest occupied molecular orbital of **I** is of a″ symmetry and is well

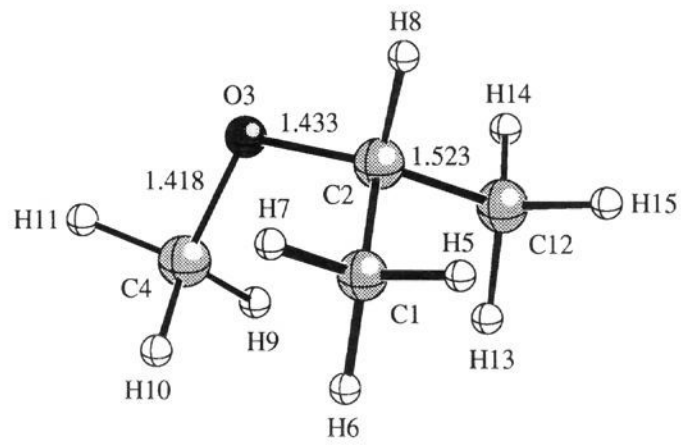

I (C_S)

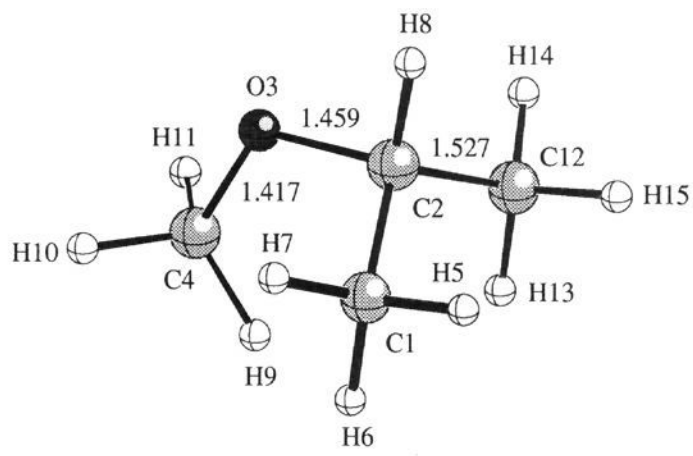

II (C_S)

Figure 1. UMP2/6-31G(d)-optimized structures in C_s symmetry of neutral (**I**) and ionized isopropyl methyl ether (**II**).

separated from the other occupied orbitals. Therefore, the equilibrium geometry of $\mathbf{1}^{\bullet+}$ was first investigated in C_s symmetry considering only the lowest $^2A''$ state. The optimized geometry of this state, **II** (Figure 1), is nearly identical to that calculated for **I**, except that the C2−O3 bond is somewhat longer and the CH_3 of the methoxy moiety has rotated about 60°. We find, however, that **II** is not a true minimum since a vibrational analysis yields 60°. We find, however, that **II** is not a true minimum since a vibrational analysis yields one imaginary frequency of $125i$ cm^{-1}, which is associated to a normal mode of a″ symmetry corresponding chiefly to a shortening of one and a lengthening of the other C−C bond of the isopropyl moiety combined with a rotation of the CH_3 of the methoxy moiety. The global minimum of $\mathbf{1}^{\bullet+}$ is found to be the C_1 structure **III** (Figure 2), which displays one slightly lengthened C−C bond of 1.578 Å. The energy of **III** relative to that of **I** (Table 1), i.e., the calculated adiabatic ionization potential of **1**, is 9.00 eV. Experimental values range from 9.42[17] to 9.50[2] eV. The higher experimental values of the adiabatic ionization potential may be due to difficulty in observing the ionization onset.

(17) Holmes, J. L.; Fingas, M.; Lossing, F. P. *Can. J. Chem.* **1981**, *59*, 80.

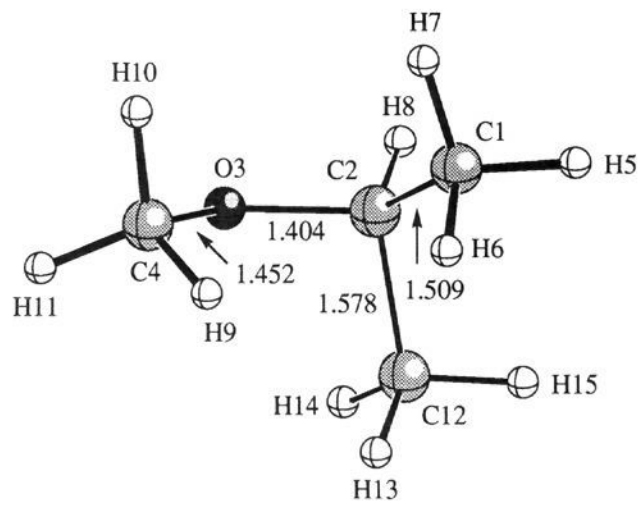

III (C_1)

Figure 2. UMP2/6-31G(d)-optimized equilibrium structure of the isopropyl methyl ether radical cation.

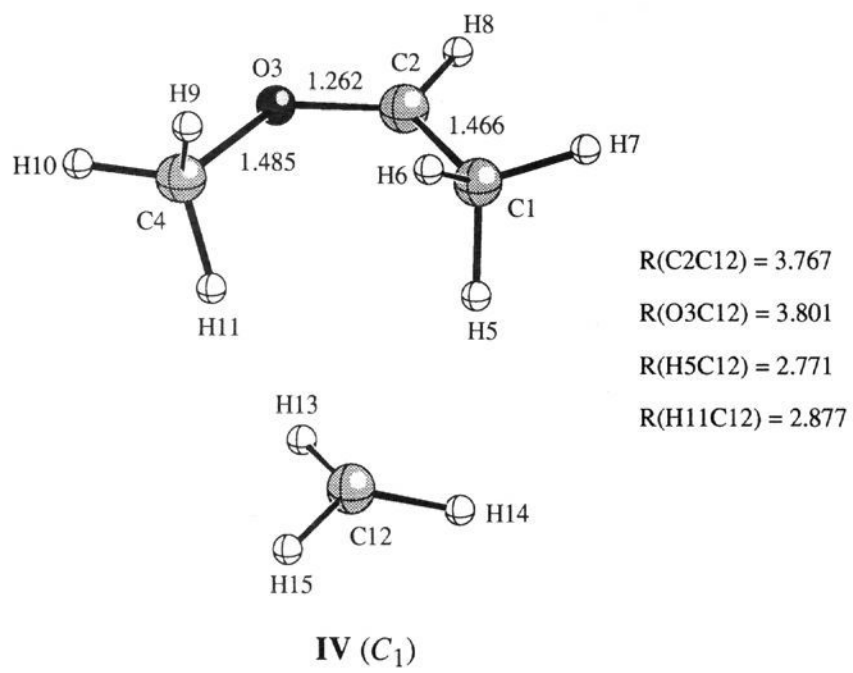

IV (C_1)

Figure 3. UMP2/6-31G(d)-optimized transition structure for the methyl migration in isopropyl methyl ether radical cation.

We elongated the C2−C12 bond of **III** systematically in steps of 0.1 Å by optimizing all other geometry parameters to simulate the minimal energy reaction path (MERP) for $CH_3^\bullet$ elimination. After a steep increase in the potential energy, reflecting the loss of covalent interaction, the methyl was found to migrate along the positively charged $CH_3CH{=}OCH_3$ moiety attracted by purely electrostatic interactions, about 3 kcal/mol below the combined energies of the separated products, $CH_3O^+{=}CHCH_3$ and $CH_3^\bullet$. The PES in that region turns out to be extremely flat, and significant geometrical changes exert practically negligible effects on the total energies. The transition structure for the methyl migration, **IV** (Figure 3), was found to have an extremely low imaginary frequency of $33i$ cm^{-1} in the corresponding vibrational analysis. Further lengthening of the C2−C12 distance in **IV** leads to the stationary point **V** (Figure 4). The force constant matrix of **V** turns out to have only positive eigenvalues and the lowest vibrational frequency of the normal modes (18 cm^{-1}) corresponds to a rotation of the methyl moiety around an axis perpendicular to the C2−O3 bond of the CH_3-$CH{=}OCH_3$ moiety rather than a methyl shift. Note that the C1−H5 bond length of structure **V** is 0.013 Å longer than in the equilibrium structure optimized for the isolated $CH_3O^+{=}CHCH_3$ ion, **VI** (Figure 4). This seems to indicate that there is a C···H bonding interaction between the hydrogen atom H5 of the $CH_3O{=}CHCH_3$ moiety and the carbon atom of the methyl moiety. The C1−H5−C12 angle of the hydrogen bridge is calculated to be 166.9°. Regarding the charge and spin density distributions (Tables 3 and 4), it is noteworthy that

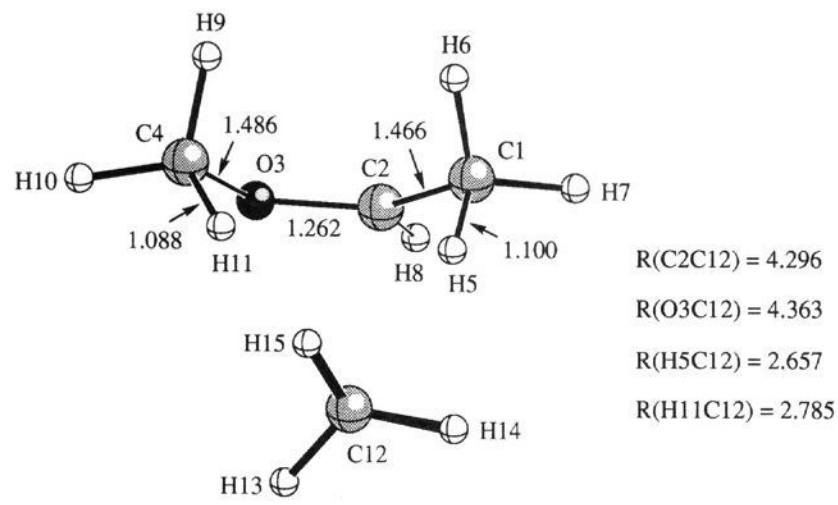

V (C_1)

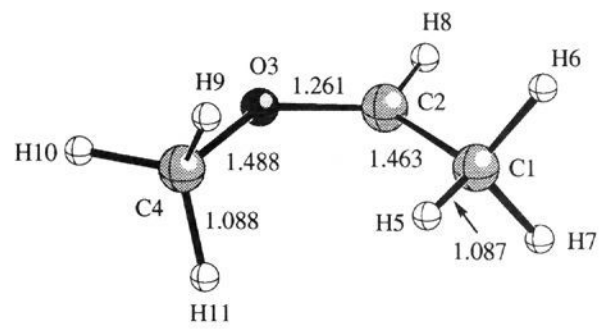

VI (C_s)

Figure 4. UMP2/6-31G(d)-optimized equilibrium structures of the ion−neutral complex $CH_3O^+{=}CHCH_3/CH_3^\bullet$ (**V**) and the $CH_3O^+{=}CHCH_3$ ion (**VI**).

the sum of the total atomic charges of the $CH_3O{=}CHCH_3$ moiety (+0.965) accounts for nearly 97% of the positive charge of **V**, whereas the sum of the total spin densities of the methyl moiety (0.965) accounts for nearly 97% of the unpaired electron population of **V**. Therefore, on the basis of the molecular geometry and the distribution of the total atomic charges and spin densities, **V** can be viewed as an ion−neutral complex between the $CH_3O^+{=}CHCH_3$ ion and the methyl radical. The energy of this complex is predicted to be 8.9 kcal/mol higher than that of the covalently bound radical cation **III** and 2.8 kcal/mol *lower* than that of its separated components, $CH_3O^+{=}CHCH_3$ and $CH_3^\bullet$. At this point we note that the endothermicity of the reaction **III** → **VI** + $CH_3^\bullet$ is calculated to be 11.7 kcal/mol, which is much larger than the reported[2] critical energy of 4.8 kcal/mol for the $CH_3^\bullet$ loss from $\mathbf{1}^{\bullet+}$. In this regard, it should be noted that the latter value was determined as the difference between the threshold (9.71 eV) for the $CH_3^\bullet$ loss from $\mathbf{1}^{\bullet+}$ and the ionization onset (9.50 eV) of **1**. However, as mentioned above, the calculated adiabatic ionization potential of **1** (9.00 eV) indicates that the observed ionization onset may correspond to a vertical ionization of **1**, rather than to its adiabatic ionization. Therefore, the previously reported critical energy of 4.8 kcal/mol for the $CH_3^\bullet$ loss from $\mathbf{1}^{\bullet+}$ probably is too low. In fact, from the available heats of formation[18] we estimate a heat of reaction of 9.6 for the dissociation of $\mathbf{1}^{\bullet+}$ into $CH_3O^+{=}CHCH_3$ and $CH_3^\bullet$, which is reasonably close to the calculated endothermicity of 11.7 kcal/mol.

With regard to the elimination of CH_4, hydrogen atom transfer must eventually occur, and, therefore, structure **V** can be viewed as a reasonable conformation within the set of various conformations of the ion−neutral complex that can interconvert within a few tenths of a kilocalorie per mole. For hydrogen transfer, i.e., covalent bond formation, the two partners of **V** should come much closer together. In fact, the C1−C12 distance in the

(18) $\Delta H^\circ_f(\mathbf{1}^{\bullet+})$ = 158.8 kcal/mol,[2] $\Delta H^\circ_f(CH_3O^+{=}CHCH_3)$ = 134.0 kcal/mol,[2] and $\Delta H^\circ_f(CH_3^\bullet)$ = −17.8[19] kcal/mol at 298 K.

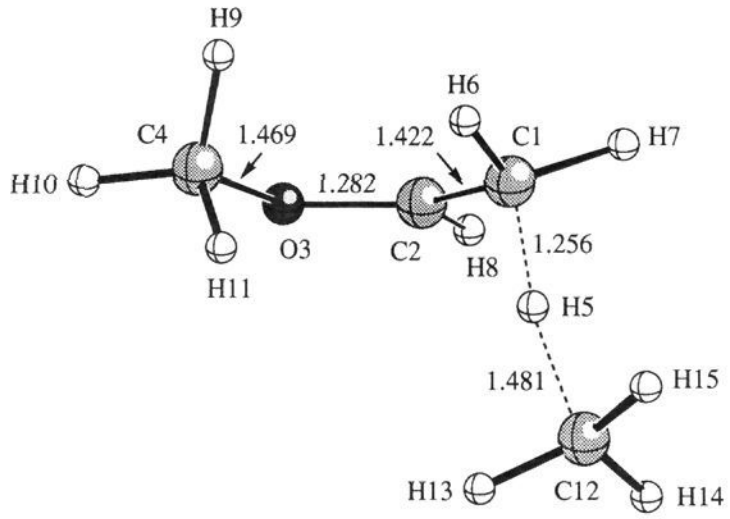

VII (C_1)

Figure 5. UMP2/6-31G(d)-optimized transition structure for the hydrogen atom transfer from an isopropyl methyl in the ion−neutral complex $CH_3O^+{=}CHCH_3/CH_3^\bullet$.

hydrogen bridge of structure **V** (3.737 Å) is substantially shortened to 2.721 Å in transition structure **VII** (Figure 5) found for the hydrogen atom transfer. The C1−H5 and C12−H5 distances of 1.256 and 1.481 Å, respectively, indicate a covalent binding of this transition structure. One important result is that the normal mode associated with the single imaginary vibrational frequency of **VII** (998*i* cm^{-1}) is dominated by a shortening of one of these two CH bonds combined with a lengthening of the other one. It can be seen from Table 2 that there is a genuine energy barrier of 4.9 kcal/mol associated with the hydrogen transfer process in **V**. The overall energy barrier for the reaction **III** → **IX** + CH_4 is predicted to be 13.8 kcal/mol, which is substantially above the critical energy of 4.4 kcal/mol reported previously[2] for the CH_4 loss from $\mathbf{1}^{\bullet+}$. Again, we note that this critical energy was determined as the difference between the threshold (9.69 eV) for the CH_4 loss from $\mathbf{1}^{\bullet+}$ and the ionization onset (9.50 eV) of **1**, assuming that the latter value corresponds to its adiabatic ionization energy. Therefore, it is likely that the reported critical energy is too low due to the adiabatic ionization energy being unobservable because of unfavorable Frank−Condon effects. In fact, combining the estimated[18] endothermicity of 9.6 kcal/mol for the dissociation of $\mathbf{1}^{\bullet+}$ into $CH_3O^+{=}CHCH_3$ and $CH_3^\bullet$ with the observed[2] difference of 0.02 eV between the onsets of $CH_3^\bullet$ loss and CH_4 loss gives an energy barrier of 9.3 kcal/mol for the CH_4 elimination from $\mathbf{1}^{\bullet+}$.

A geometry reoptimization of **VII**, slightly modified according to this normal mode with the appropriate sign, leads to a local minimum, **VIII** (Figure 6), which appears to be a weakly bound ion−neutral complex between the methyl vinyl ether radical cation ($CH_3OCH{=}CH_2^{\bullet+}$) and methane. Thus the charge and spin density distributions (Tables 3 and 4) indicate that the methyl vinyl ether moiety accounts for nearly 100% of both the positive charge and unpaired electron population of **VIII**. Furthermore, the geometrical parameters of the methyl vinyl ether partner of structure **VIII** are nearly identical to those of the equilibrium structure optimized for the isolated methyl vinyl radical cation, **IX** (Figure 6). The ion complex **VIII** is stabilized by 1.7 kcal/mol toward decomposition into its loosely bound components. Since BSSE are expected to affect the computed interaction in the electrostatically bound complex **VIII**, the latter stabilization energy value should be taken with caution. On the other hand, the endothermicity of 1.0 kcal/mol predicted for the reaction **III** → **IX** + CH_4 is reasonably close to the

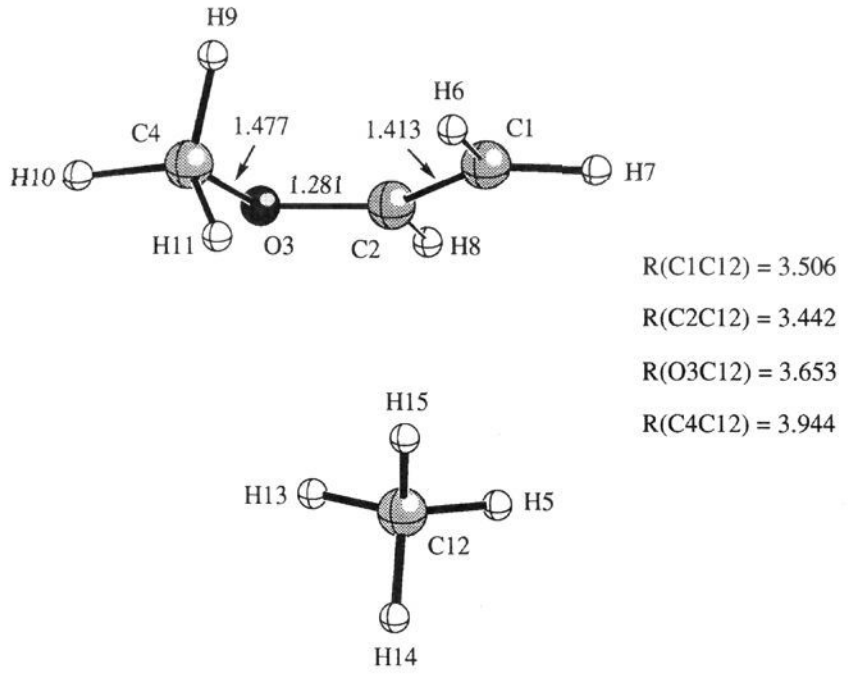

VIII (C_1)

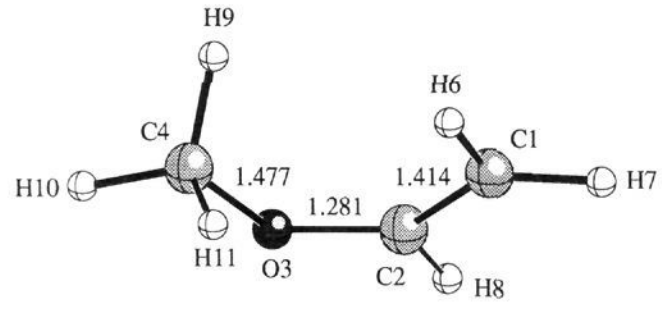

IX (C_S)

Figure 6. UMP2/6-31G(d)-optimized equilibrium structures of the ion−neutral complex $CH_3OCH{=}CH_2^{\bullet+}/CH_4$ (**VIII**) and the CH_3-$OCH{=}CH_2^{\bullet+}$ radical cation (**IX**).

experimental estimate[20] of 3.5 kcal/mol for the decomposition of $\mathbf{1}^{\bullet+}$ into methyl vinyl radical cation and methane.

For the sake of completeness, the alternative hydrogen atom H11 transfer in the ion−neutral complex structure **V** has also been studied. Such a hydrogen shift is predicted to take place through transition structure **X** (Figure 7). The C4−H11 and C12−H11 distances of 1.358 and 1.306 Å, respectively, again indicate a covalent binding of this transition structure. The normal mode associated with the single imaginary vibrational frequency of **X** (1822*i* cm^{-1}) corresponds chiefly to a shortening of one of these two CH bonds and a lengthening of the other one. The energy of saddle point **X** is predicted to be 10.0 kcal/mol higher than that of **VII**. Furthermore, the hydrogen atom transfer through transition structure **X** leads to a radical cation, i.e., $CH_3CH{=}OCH_2^{\bullet+}$, whose optimized equilibrium structure **XI** (Figure 7) is predicted to be 8.5 kcal/mol more energetic than its isomeric structure **IX**. These theoretical results reproduce the experimental observation that the additional hydrogen atom in the methane eliminated from $\mathbf{1}^{\bullet+}$ comes exclusively from the isopropyl methyls.[2]

Alternatively, the ion−neutral complex intermediate **V** may decompose into its components, $CH_3O^+{=}CHCH_3$ and $CH_3^\bullet$, in a continuously endothermic process. At this point we note that these dissociation products are 2.1 kcal/mol *below* transition structure **VII** for the lowest energy hydrogen atom transfer channel in **V**. However, only CH_4 loss has been observed for metastable ions $\mathbf{1}^{\bullet+}$.[2,3] While this reaction is predicted to be 10.7 kcal/mol less endothermic than the elimination of $CH_3^\bullet$, it is kinetically disfavored due to the barrier of 13.8 kcal/mol calculated for the CH_4 elimination from structure **III**. In order

(19) Lias, S. G.; Bartmess, J. E.; Liebman, J. B.; Holmes, J. L.; Levin, R. D.; Mallard, W. G. *J. Phys. Chem. Ref. Data* **1988**, *17*, 168.

(20) Estimated from $\Delta H°_f(\mathbf{1}^{\bullet+})$ = 158.8 kcal/mol,[2] $\Delta H°_f(CH_3OCH{=}CH_2^{\bullet+})$ = 180.1 kcal/mol,[2] and $\Delta H°_f(CH_4)$ = −17.8[19] kcal/mol at 298 K.

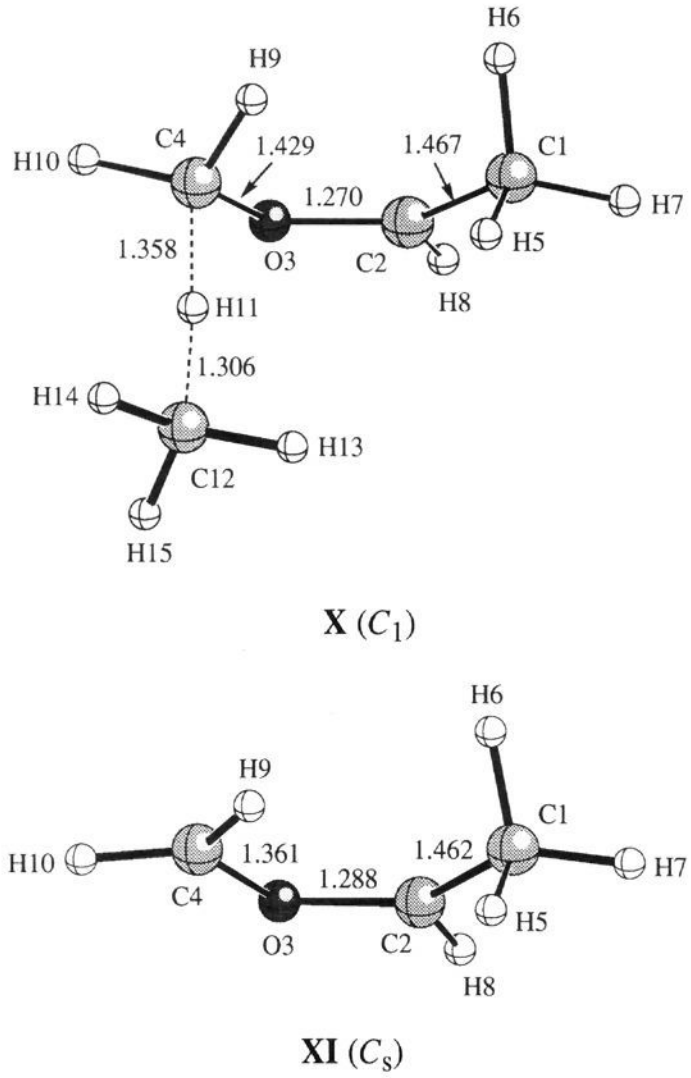

Figure 7. UMP2/6-31G(d)-optimized transition structure for the hydrogen atom transfer from the methoxy methyl in the ion−neutral complex CH_3O^+=$CHCH_3/CH_3^\bullet$ (**X**) and UMP2/6-31G(d)-optimized equilibrium structure of the CH_3CHO=$CH_2^{\bullet+}$ radical cation (**XI**).

to solve this problem, we have performed calculations of the unimolecular rate constant by using RRKM theory. The results will be described in the next section.

RRKM Computational Details

For both CH_4 and $CH_3^\bullet$ losses from **1**, the dependence of the unimolecular rate constant $k(E)$ on the internal energy E of a reactant ion was initially calculated on the basis of standard RRKM theory of unimolecular reactions, which can be formulated as[22]

$$k(E) = \frac{\sigma W^\dagger(E)}{h\varrho(E)} \tag{1}$$

where σ is the reaction path degeneracy, $W^\dagger(E)$ is the total number of states of the transition state with energy less than or equal to E, $\varrho(E)$ is the density of states of the reactant ion, and h is Planck's constant. $W^\dagger(E)$ and $\varrho(E)$ were enumerated by direct count of vibrational states using a program[23] based on the Beyer−Swinehart algorithm.[22,24]

The RRKM computations employed the potential energy barriers calculated at the QCISD(T)/6-31G(d,p) level and the UMP2/6-31G(d)-calculated harmonic vibrational frequencies scaled by the factor 0.93. Reactant frequencies were taken equal to those calculated for equilibrium structure **III**. For CH_4 elimination, the relative energy of 17.5 kcal/mol calculated for **VII** was taken as the barrier height and the harmonic vibrational frequencies calculated for this transition structure were taken as the transition-state frequencies. For $CH_3^\bullet$ loss, the relative energy of 15.8 kcal/mol calculated at the QCISD(T)/6-31G(d,p) level for the dissociation fragments was taken as the barrier height of this reaction, whereas the harmonic vibrational frequencies calculated for the ion−neutral intermediate **V** were taken as the transition-state frequencies. One of these, 106 cm^{-1}, corresponding to the C1−H5−C12 stretching mode, was chosen as the reaction coordinate frequency.[25]

In addition, the possibility of a hydrogen transfer via quantum-mechanical barrier tunneling (QMBT) was investigated for the CH_4 elimination. This possibility, aimed at resolving the discrepancies between experiment and theory, was based on the aforementioned observation that the main contribution to the reaction coordinate of **VII**, i.e., the normal mode associated to the imaginary frequency, is from the migrating hydrogen atom. Furthermore, it has been proposed that CH_4 elimination from the acetone radical cation proceeds by a QMBT mechanism.[25] To incorporate QMBT effects in the framework of the RRKM theory,[26] $W^\dagger(E)$ in eq 1 was replaced by $W_{QM}{}^\dagger(E)$:

$$W_{QM}{}^\dagger(E) = \sum P(E - \epsilon_n{}^\dagger) \tag{2}$$

where $P(E)$ is the one-dimensional tunneling probability as a function of the energy E in the reaction coordinate and $\epsilon_n{}^\dagger$ is the vibrational energy levels of the transition state; in the classical limit of no tunneling $W_{QM}{}^\dagger(E) \rightarrow W^\dagger(E)$. The barrier along the reaction coordinate was approximated by a generalized Eckart potential[27] with tunneling taking place between the reactant ion **III** and the ion−neutral complex **VIII**. The heights adopted for the Eckart barrier are $V_1 = 17.5$ kcal/mol and $V_2 = 16.5$ kcal/mol, respectively (see Table 2).

To investigate whether the sorts of changes in vibrational frequencies calculated for transition structure **VII** are of the right magnitude to account for the observed[2] large primary isotope effects associated with

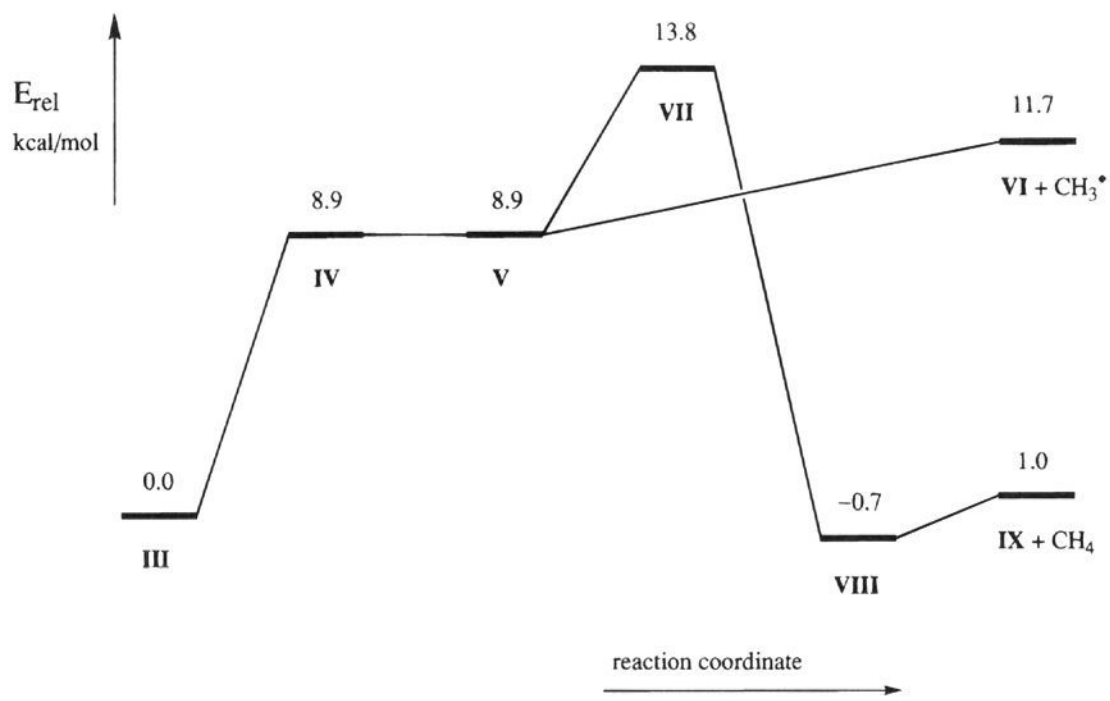

Figure 8. Schematic potential energy diagram showing the unimolecular decompositions of ionized isopropyl methyl ether. Energy values obtained from the ZPVE-corrected QCISD/6-31G(d,p) energies relative to that of **III**.

Table 5. RRKM-Calculated Rate Constants (k, s^{-1}) as a Function of the Internal Energy (E, kcal/mol) for Losses of Methane and Methyl Radical from Ionized Isopropyl Methyl Ether

	$k(CH_4)$		
E^a	classical	QMBT[b]	$k(CH_3^{\bullet})$
11.4	0	9.48×10^4	0
11.5	0	1.14×10^5	0
11.6	0	1.38×10^5	0
11.7	0	1.66×10^5	4.78×10^5
11.8	0	1.99×10^5	1.77×10^6
11.9	0	2.40×10^5	4.49×10^6
12.0	0	2.88×10^5	9.04×10^6
12.1	0	3.46×10^5	1.63×10^7
12.2	0	4.15×10^5	2.74×10^7
12.3	0	4.99×10^5	4.30×10^7
12.4	0	5.97×10^5	1.63×10^7
12.5	0	7.16×10^5	9.41×10^7
13.0	0	1.73×10^6	4.21×10^8
13.7	0	5.57×10^6	1.89×10^9
13.8	0.96×10^5	6.52×10^6	2.26×10^9
13.9	1.78×10^5	7.60×10^6	2.68×10^9
14.0	4.13×10^5	8.84×10^6	3.16×10^9

[a] Internal energy relative to the ZPVE of the radical cation. [b] Rate constants calculated including quantum-mechanical barrier tunneling.

CH_2D_2 and CHD_3 losses from metastable **1a**$^{\bullet+}$, the unimolecular rates of decomposition for this D_4-labeled radical cation were calculated on the basis of RRKM theory including QMBT. It should be noted that, due to the differences in the calculated ZPVE of the transition states involved, the barrier heights calculated for the CH_2D_2 and CHD_3 losses from metastable **1a**$^{\bullet+}$ are 14.1 and 15.0 kcal/mol, respectively, compared to the barrier height of 13.8 kcal/mol calculated for CH_4 loss from metastable **1**$^{\bullet+}$. For the same reason, the endothermicity calculated for the dissociation of **1a**$^{\bullet+}$ into CH_3O^+=$CHCHD_2$ and $CDH_2^{\bullet}$ is calculated to be 12.6 kcal/mol, compared to the value of 11.7 kcal/mol calculated for the dissociation of **1**$^{\bullet+}$.

Results and Discussion of the RRKM Calculations

Table 5 summarizes the unimolecular rate constant $k(CH_4)$ and $k(CH_3^{\bullet})$ for losses of methane and methyl radical as a function of the internal energy E (relative to the ZPVE of **1**$^{\bullet+}$). Regarding CH_4 elimination, the first column gives the classical rate constants (no QMBT), whereas the second one shows the rate constants calculated including QMBT. As expected, the classical rate constant for CH_4 elimination vanishes at energies below 13.8 kcal/mol (the transition structure **VII** barrier height), so $CH_3^{\bullet}$ loss is the only reaction taking place. Incorporation of QMBT in the RRKM calculations of the unimolecular rate constant for the CH_4 elimination reaction changes dramatically the decomposition pattern at energies below the threshold (11.7 kcal/mol) for $CH_3^{\bullet}$ loss. Thus the QMBT effects allow CH_4 elimination to take place below the barrier height for transition structure **VII**. Within the narrow internal energy range 11.4–11.6 kcal/mol, CH_4 elimination is the only reaction taking place. Furthermore, its calculated rate constants are in the range 0.9×10^5 to 1.4×10^5. Therefore, it is not surprising that it produces a metastable decomposition. It can be seen that at 11.7 kcal/mol $CH_3^{\bullet}$ loss is about 3 times faster than CH_4 elimination, which from that point onward, with increasing internal energies, is completely suppressed. These findings are in good agreement with the experimental observation that the onsets for the two reactions differ by only a few tenths of a kilocalorie per mole.[2]

Table 6. RRKM-Calculated Rate Constants (k, s^{-1}) and Rate-Constant Ratios as a Function of the Internal Energy (E, kcal/mol) for Losses of CH_2D_2 and CHD_3 from Metastable $CH_3OCH(CHD_2)_2^{\bullet+}$

E^a	$k(CH_2D_2)$	$k(CHD_3)$	$k(CH_2D_2)/k(CHD_3)$
12.3	8.97×10^4	1.40×10^3	64.1
12.4	1.08×10^5	1.80×10^3	60.0
12.5	1.31×10^5	2.32×10^3	56.5

[a] Internal energy relative to the ZPVE of the metastable radical cation.

Table 6 summarizes the unimolecular rate constants $k(CH_2D_2)$ and $k(CHD_3)$ and the corresponding rate-constant ratios $k(CH_2D_2)/k(CHD_3)$ for the methane loss from metastable **1a**$^{\bullet+}$ as a function of the internal energy E in the range 12.3–12.5 kcal/mol. This energy range was determined as the internal energies below the threshold (12.6 kcal/mol) for $CHD_2^{\bullet}$ loss which are necessary to eliminate CH_2D_2 with a rate constant of about 10^5 s^{-1}. Recalling that the barrier heights calculated for the CH_2D_2 and CHD_3 losses from metastable **1a**$^{\bullet+}$ are 14.1 and 15.0 kcal/mol, respectively, it turns out that within the selected energy range these reactions cannot occur without quantum-mechanical tunneling. It is readily noticeable from Table 6 that the $k(CH_2D_2)/k(CHD_3)$ rate-constant ratio predicted at the internal energy of 12.4 kcal/mol exactly reproduces the experimental primary isotope effect of 60.[2] This theoretical result provides a good test of the reliability of the transition structure (**VII**) predicted for the methane elimination from **1**$^{\bullet+}$. Furthermore, it lends strong support to our contention that the hydrogen atom transfer in the ion–neutral complex intermediate **V** involves quantum-mechanical tunneling through a potential energy barrier. At this point it should be mentioned that in a recent article Osterheld and Brauman[28] disputed the conclusion of Schwarz and co-workers[25] that the CH_4 elimination from ionized acetone proceeds by a tunneling mechanism. We think that **1**$^{\bullet+}$ is a better system to address this issue than is the acetone radical cation, because in the latter the products of CH_4 and $CH_3^{\bullet}$ losses are found to be very close in energy (i.e., the two products differ by *ca.* 1 kcal/mol[29]), so it is not clear that a barrier must be surmounted on the reaction path to CH_4 elimination. In contrast, there clearly must be a barrier to CH_4 elimination from **1**$^{\bullet+}$. Therefore, our work provides a convincing example for tunneling through a genuine barrier in ionic fragmentation processes.

Conclusions

Our computational exploration of the $C_4H_{10}O^{\bullet+}$ potential energy surface in the regions concerning the $CH_3^{\bullet}$ and CH_4 losses from ionized isopropyl methyl ether reveals several important points:

(1) The equilibrium geometry of the ground state isopropyl methyl ether radical cation is predicted to be a C_1 structure showing one slightly lengthened C–C bond of 1.578 Å.

(2) Dissociation of the isopropyl methyl ether radical cation leads to methyl radical loss, but the methyl radical is attracted by an ion–induced dipole attraction to the CH_3O^+=$CHCH_3$

(21) Derived from the endothermicity of 9.6 kcal/mol estimated[18] for the dissociation of **1**$^{\bullet+}$ into CH_3O^+=$CHCH_3$ plus $CH_3^{\bullet}$, and the difference of 0.5 ± 0.2 kcal/mol between the photoionization appearance energies for the products of CH_4 and $CH_3^{\bullet}$ eliminations.[2]

(22) Gilbert, R. G.; Smith, S. C. *Theory of Unimolecular and Recombination Reactions*; Blackwell Scientific Publications: Oxford, 1990.

(23) Solé, A., unpublished work.

(24) Beyer, T.; Swineheart, D. F. *Comm. Assoc. Comput. Machines* **1973**, *16*, 379.

(25) Heinrich, N.; Louage, F.; Lifshitz, C.; Schwarz, H. *J. Am. Chem. Soc.* **1988**, *110*, 8183.

(26) (a) Miller, W. H. *J. Am. Chem. Soc.* **1979**, *101*, 6810. (b) Garrett, B. C.; Truhlar, D. G. *J. Phys. Chem.* **1979**, *83*, 1079.

(27) Johnston, H. S. *Gas Phase Reaction Rate Theory*; Ronald Press: New York, 1966.

(28) Osterheld, T. H.; Brauman, J. I. *J. Am. Chem. Soc.* **1992**, *114*, 7158.

(29) Traeger, J. C.; Hudson, C. E.; McAdoo, D. J. *J. Phys. Chem.* **1988**, *92*, 1519.

cation below its dissociation limit forming an ion−neutral complex intermediate.

(3) The methyl radical partner of the ion−neutral complex may move to the other isopropyl methyl group of the $CH_3O^+{=}CHCH_3$ partner and abstract a hydrogen atom. There is a genuine energy barrier of about 5 kcal/mol associated with this hydrogen atom transfer.

(4) Alternatively, the ion−neutral complex may decompose into its loosely bound components, $CH_3O^+{=}CHCH_3$ and $CH_3^\bullet$, in a continuously endothermic process. The dissociation products are about 2 kcal/mol below the transition structure found for hydrogen atom transfer.

(5) The hydrogen atom transfer in the ion−neutral complex can only take place below the top of its energy barrier and dominates at internal energies beneath the methyl radical dissociation limit due to quantum-mechanical tunneling through a potential energy barrier.

(6) The observed large primary isotope effects associated with CH_2D_2 and CHD_3 losses from metastable D_4-labeled radical cation are attributed to a combined effect of the changes in zero-point vibrational energies of the transition structure involved in the hydrogen or deuterium atom transfer and the differences in the one-dimensional tunneling probability shown by these two atoms.

Acknowledgment. This work was supported by the Robert A. Welch foundation (Grant Nos. H-609 and BD-1106) and the Spanish DGICYT (Grant No. PB92-0796-C02-01). The preliminary UHF calculations were carried out by one of us (S.O.) in the Department of Marine Sciences (Texas A&M University at Galveston), during his stay in the summer of 1991, which was partially supported by the Catalonian CIRIT foundation. We acknowledge the University of Texas Center for High Performance Computing and the Centre de Supercomputació de Catalunya for generous allocations of computing time. We also acknowledge helpful discussions with Dr. Charles Hudson from the Marine Biomedical Institute.

Supplementary Material Available: **Z** matrices of the MP2/6-31G(d)-optimized geometries for structures **I**−**XI** (7 pages). This material is contained in many libraries on microfiche, immediately follows this article in the microfilm version of the journal, can be ordered from the ACS, and can be downloaded from the Internet; see any current masthead page for ordering information and Internet access instructions.

JA943366I